



Corrosion behaviour of additively manufactured 316L and CoCrNi

Downloaded from: <https://research.chalmers.se>, 2025-12-04 23:23 UTC



Citation for the original published paper (version of record):

Malladi, B., Tam, E., Cao, Y. et al (2023). Corrosion behaviour of additively manufactured 316L and CoCrNi. *Surface and Interface Analysis*, 55(6-7): 404-410. <http://dx.doi.org/10.1002/sia.7200>

N.B. When citing this work, cite the original published paper.

RESEARCH ARTICLE

Corrosion behaviour of additively manufactured 316L and CoCrNi

Sri Bala Aditya Malladi  | Pui Lam Tam | Yu Cao  | Sheng Guo | Lars Nyborg 

Department of Industrial and Materials Science, Chalmers University of Technology, Gothenburg, Sweden

Correspondence

Sri Bala Aditya Malladi, Department of Industrial and Materials Science, Chalmers University of Technology, Gothenburg, Sweden.

Email: malladi@chalmers.se

Funding information

Swedish Innovation Agency, Grant/Award Number: 2016-05175; European Union's Horizon 2020, Grant/Award Number: 820774

Alloys such as 316L and the medium-entropy alloy CoCrNi are known for their excellent strength and corrosion properties. In the present study, bulk samples of 316L and CoCrNi (without and with 0.11 wt.% N) alloys fabricated using powder bed fusion laser beam (PBF-LB) were tested in the as-printed state for their corrosion behaviour in 0.5 M H₂SO₄ without and with added 3 wt.% NaCl. The tests were done using potentiodynamic measurements and the results were compared with those of the conventionally manufactured 316L. By means of angle-resolved X-ray photoelectron spectroscopy (ARXPS), the passive film characteristics were studied in terms of composition and film thickness. The 316L fabricated using PBF-LB showed favourable passivation and corrosion behaviour as compared with its conventionally manufactured counterpart. It was observed that all the alloys fabricated using the PBF-LB showed similar corrosion behaviour, but with CoCrNi and CoCrNi-N showing better passivation behaviour than 316L alloys in the presence of NaCl. The ARXPS showed the presence of both hydroxide and oxides in all the alloys, with outer hydroxide layer and inner oxide layer. The ARXPS of both 316L alloys showed the expected presence of Cr-Fe oxide on the surface of as-passivated samples, whereas the presence of sulphide was also depicted for the conventionally manufactured 316L, supposed to be detrimental to its corrosion behaviour. The CoCrNi-based alloys showed the presence of only Cr₂O₃ layer in their passivated state, with Co and Ni acting as noble elements in the formation of the passive film. Upon micro-alloying with the strong solid solution strengthener N, CoCrNi did not show any negative effect on either the corrosion behaviour or the passivation behaviour of the alloy.

KEYWORDS

additive manufacturing, corrosion behaviour, medium-entropy alloy, powder bed fusion-laser beam, stainless steel, X-ray photoelectron spectroscopy

1 | INTRODUCTION

Additive manufacturing (AM) processes refer to the processes that manufacture components layer by layer to near net shape in a bottom-up approach, as opposed to the traditional top-down subtractive manufacturing processes.^{1,2} Among the AM techniques, powder

bed fusion-laser beam (PBF-LB) uses high-power laser to rapidly melt and solidify thin layers of powder selectively and rapidly. Once a layer of material is selectively fused, a new layer of material is applied, and the process is repeated until a three-dimensional component with near net shape and nominally full densification is produced.¹⁻³ Due to the inherent high thermal gradient and solidification rate, the

This is an open access article under the terms of the [Creative Commons Attribution](https://creativecommons.org/licenses/by/4.0/) License, which permits use, distribution and reproduction in any medium, provided the original work is properly cited.

© 2023 The Authors. *Surface and Interface Analysis* published by John Wiley & Sons Ltd.

resulting microstructure of the PBF-LB components typically consists of the epitaxially grown columnar grains and is unlike the microstructure of the components produced by traditional manufacturing techniques.^{4–10}

The ability to produce the parts on-demand, with near-full-densification and near-net-shape components, makes PBF-LB a desirable technique for industrial applications. With the growing material portfolios of PBF-LB, there is also growing interest in the wide range of properties for the materials, and one such properties is the corrosion behaviour of the alloys.^{11–13} The focus on the corrosion properties of the alloys manufactured through PBF-LB has been mainly on Al-based, Fe-based and Ti-based alloy systems.^{11,12}

Among the Fe-based alloys, 316L is the most studied alloy for its corrosion properties with studies mainly focusing on understanding the influence of the microstructure, porosity and inclusions on the corrosion behaviour. When compared with the wrought variant of 316L, the PBF-LB variant typically showed better corrosion resistance mainly owing to its unique microstructure and rapid solidification rate, which suppresses the formation of undesirable inclusions that are detrimental to the corrosion performance.^{14–16} The porosity of the parts is also an important aspect when it comes to the corrosion properties of the alloys, specifically considering the re-passivation behaviour. Studies on the influence of the porosity of the PBF-LB parts show that pore characteristics such as pore shape, size and distribution seem to heavily influence the pitting behaviour of the alloys.^{11,12,17} With the present state of the art, the PBF-LB 316L provides nominally pore-free materials; see, for example, ref.^{18–20}

High-entropy alloys (HEAs) and medium-entropy alloys (MEAs) are members of the novel class of alloys that comprise several principal elements in nearly equiatomic proportions. These alloys have attained increased interest over the last two decades due to their excellent mechanical properties and damage tolerance.^{21–25} With increasing interest in this novel class of alloys, there is also increasing interest in understanding their corrosion behaviour. Due to the compositional complexity of these alloys, the corrosion behaviour will also vary based on the alloying elements in these alloys. In case of the single-phase face-centred cubic HEAs, the presence of high amount of Cr is known to significantly enhance the corrosion behaviour of the alloys.²⁶ Similarly, addition of elements such as Al, Ti, Mo, B and N is also known to further enhance the corrosion resistance of HEAs.²⁷ The corrosion behaviour of HEAs were reportedly either comparable or in most cases better than the stainless steels. Although there are increased efforts on the development of HEAs and MEAs using AM, very limited studies are available on the corrosion behaviour of these alloys, especially in comparison with their stainless steel counterparts.

Equiatomic CoCrNi is one of the most widely studied MEA owing to its excellent strength, ductility, oxidation and corrosion resistance, enhanced hydrogen embrittlement resistance and excellent cryogenic mechanical properties.^{28–30} Addition of nitrogen as an interstitial is known to not only improve the strength but also to improve the corrosion behaviour of the wrought CoCrNi MEA.²⁸ The improved corrosion performance of the nitrogen-containing MEA was attributed to the presence of relatively higher fraction of oxides/hydroxides on the

surface. With relatively higher Cr content as compared with the stainless steels, combined with the better mechanical properties, these alloys could be engineered to potentially perform better than traditional 316L in the corrosive environment.

The aim of this study is to understand, compare and benchmark the corrosion and passivation behaviour of CoCrNi and CoCrNi-N (0.11 wt.% N) manufactured by PBF-LB, with 316L (AM and conventionally manufactured). Conventional 316L is one of the most commonly used alloys in the field of marine engineering.^{31–33} However, the conventional 316L is also susceptible to pitting corrosion in the saline environments owing to the presence of MnS inclusions though the absence of such precipitates in additively manufactured 316L is known to result in the improved pitting resistance.^{14,15,34,35} The testing approach includes potentiodynamic polarisation studies in sulphuric acid without and with sodium chloride addition to simulate and understand their behaviour in the acidic and saline environments. Detailed investigations of synthetically passivated samples using X-ray photoelectron spectroscopy (XPS) were performed to depict the correlation between the passivation behaviour and the passive film chemistry of the MEAs and stainless steels.

2 | MATERIALS AND METHODS

2.1 | Materials

The materials used in the present study are shown in Table 1. The PBF-LB fabrication of 316L and CoCrNi and CoCrNi-N was performed using the EOS M100 machine equipped with 200 W Yb-fibre laser, with a focus diameter of 40 μm . In all cases, pre-alloyed powder in the size range of 20–50 μm supplied by Höganäs AB, were used for the studies. Cylindrical samples of 12 mm in diameter and 30 mm in height were printed in the vertical orientation with optimised parameters, yielding relative densities greater than 99.9% in all cases. As a benchmark, conventional 316L of same dimensions was prepared from extruded and machined rod specimens. Samples manufactured by PBF-LB and conventional routes were machined to the shape of cylindrical discs with a diameter of 10 mm and thickness of 2 mm. The machined samples were ground down to 4000 grits SiC paper followed by fine polishing using 3 and 1 μm suspended diamond solutions. All materials are fully austenitic and expected to contain oxide inclusions,⁹ and the conventional 316L is expected to also contain manganese sulphide inclusions.³⁴

TABLE 1 List of studied materials and their manufacturing route.

Material	Manufacturing route
316L	PBF-LB
316L	Conventional
CoCrNi	PBF-LB
CoCrNi-N (0.11 wt.% of N)	PBF-LB

2.2 | Electrochemical studies

The electrochemical tests were performed on all the materials in 0.5 M H_2SO_4 and 0.5 M H_2SO_4 + 3 wt.% NaCl solutions to study the corrosion behaviour of 316L (manufactured by both conventional route and PBF-LB) and MEAs (manufactured by PBF-LB). The tests in both solutions were carried out by means of three-electrode setup using the Solatron 1287 potentiostat. The fine-polished cylindrical samples were cleaned and mounted in a Teflon sample holder as the working electrode with $\sim 0.5 \text{ cm}^2$ of area exposed to the solution. This set-up was connected to a platinum auxiliary electrode and silver/silver chloride (Ag/AgCl) reference electrode. Prior to the polarisation experiments, the electrochemical cell was purged with nitrogen (5 N purity) for 60 min, and the open circuit potential (E_{OCP}) was monitored until it stabilised. To obtain the potentiodynamic polarisation plots, the potential was then set to -0.5 V (vs. E_{OCP}) and then increased to the final value of $+1.2 \text{ V}$ (vs. E_{OCP}) at a scan rate of 2 mVs^{-1} . To understand the passivation behaviour of the materials, the similar potentiodynamic set-up was used and the potential was varied between -0.5 (vs. E_{OCP}) and 0.5 V (vs. E_{OCP}) in 0.5 M H_2SO_4 + 3 wt.% NaCl to reach the passivation region for all the materials. The as-passivated samples were then taken to angle-resolved XPS (ARXPS) for analysis of the passive film. The corrosion currents (I_{corr}) were measured using the linear extrapolation from the cathodic Tafel region.

2.3 | XPS studies

XPS analysis on as-passivated samples was conducted by using the PHI 5000 Versaprobe III instrument equipped with monochromatic

AlK_{α} X-ray source ($E = 1486.6 \text{ eV}$), with a beam diameter of $100 \mu\text{m}$ and under ultra-high vacuum of 10^{-9} mbar . Before the measurements, calibration of the instrument was carried out using $\text{Au}4f^{7/2}$ (83.96 eV), $\text{Ag}3d^{5/2}$ (368.21 eV) and $\text{Cu}2p^{3/2}$ (932.62 eV) peaks, according to ISO 15472. Survey scans were performed between 0 and 1250 eV binding energy with a step size of 1.0 eV to evaluate the overall compositions. ARXPS was done at take-off angles of 30° , 45° and 60° relative to the sample surface on all the alloys that were passivated up to 0.5 V (vs. E_{OCP}) to understand the passivation behaviour of the materials. The narrow scan measurements and the ARXPS measurements were aligned with the adventitious carbon peak ($\text{C}1s$) at 284.8 eV for all the samples for analysis. Iterated Shirley-type background correction was applied as it is necessary to remove the peaks from an inelastic scattering background, and asymmetric components were assigned for the area integration.

3 | RESULTS AND DISCUSSION

3.1 | Potentiodynamic polarisation measurements

The potentiodynamic polarisation plots obtained from the electrochemical corrosion tests performed on 316L (conventional and PBF-LB), CoCrNi and CoCrNi-N alloys in 0.5 M H_2SO_4 and 0.5 M H_2SO_4 + 3 wt.% NaCl are shown in Figure 1. The measured corrosion potentials and corrosion current densities are presented in Table 2.

As compared with the conventionally manufactured 316L, the PBF-LB 316L shows higher free corrosion potential (E_{corr}) and smaller corrosion current density (I_{corr}) in both environments. Also, the passivation current density is observed to be significantly smaller for the

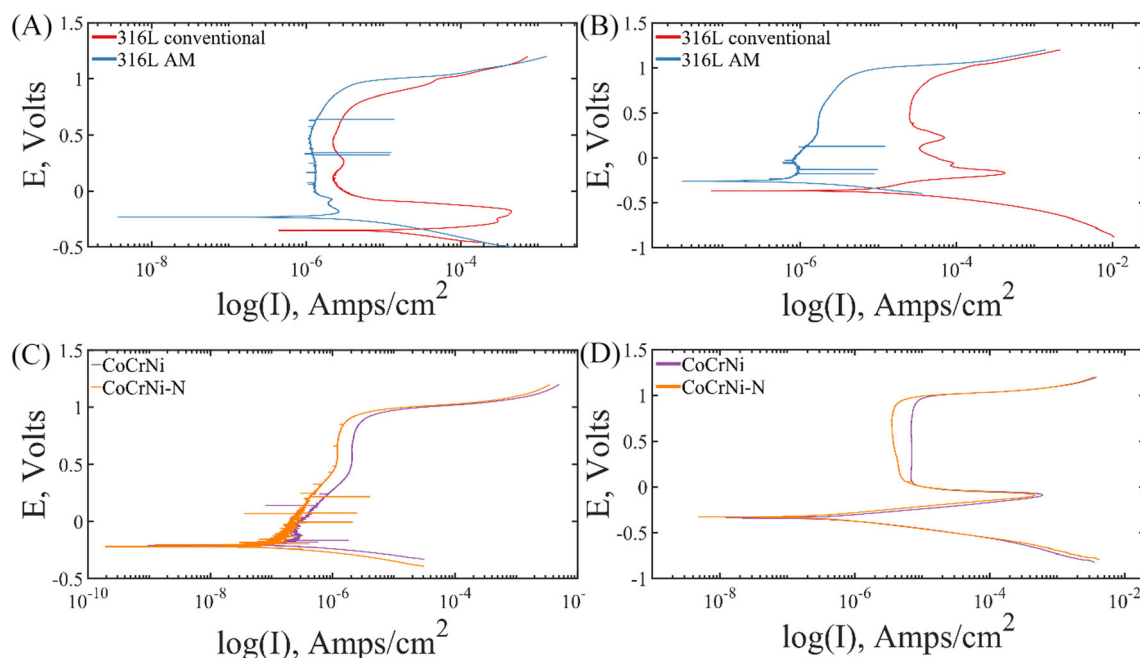


FIGURE 1 Potentiodynamic polarisation plots for 316L (conventional and AM) in (A) 0.5 M H_2SO_4 , (B) 0.5 M H_2SO_4 and 3 wt.% NaCl and MEAs (CoCrNi and CoCrNi-N) in (C) 0.5 M H_2SO_4 and (D) 0.5 M H_2SO_4 and 3 wt.% NaCl.

TABLE 2 Corrosion potentials (E_{corr}) and corrosion current densities (I_{corr}) extrapolated from the cathodic Tafel plots, obtained from potentiodynamic polarisation tests.

Environment		316L conventional	316LPBF-LB	CoCrNiPBF-LB	CoCrNi-NPBF-LB
0.5 M H ₂ SO ₄	E_{corr}	−0.35	−0.23	−0.20	−0.21
	I_{corr}	1.1×10^{-05}	4.0×10^{-06}	4.2×10^{-07}	4.3×10^{-07}
0.5 M H ₂ SO ₄ and 3 wt.% NaCl	E_{corr}	−0.36	−0.26	−0.33	−0.32
	I_{corr}	2.8×10^{-04}	1.5×10^{-06}	6.9×10^{-07}	5.6×10^{-07}

316L manufactured using PBF-LB (Figure 1). These results suggest that the PBF-LB 316L has better corrosion resistance as compared with its wrought counterpart, as has been observed by Chao et al.³⁶ This improved corrosion resistance in the 316L manufactured using PBF-LB was attributed to the fast solidification rate, which suppresses the formation of phases, which could be detrimental to the corrosion behaviour of these alloys.

The potentiodynamic curves of PBF-LB CoCrNi and CoCrNi-N for 0.5 M H₂SO₄ and 0.5 M H₂SO₄ + 3 wt.% NaCl are shown in Figure 1C,D. In 0.5 M H₂SO₄, both MEAs show pseudo-passivation before reaching the transpassive region, but when the MEAs are tested in 0.5 M H₂SO₄ + 3 wt.% NaCl, passivation is observed. The transpassive behaviour of both alloys is observed to be similar in both 0.5 M H₂SO₄ and 0.5 M H₂SO₄ + 3 wt.% NaCl. E_{corr} of both alloys are observed to be very similar, whereas slightly smaller I_{corr} is observed for CoCrNi-N as compared with CoCrNi. Overall, the potentiodynamic behaviour is observed to be very similar for these two alloys in the observed polarisation plots. These observations are, however, quite different as compared with the observations made by Moravick et al.,²⁸ who observed improved corrosion response of wrought CoCrNi MEAs with the addition of 0.5 wt.% of nitrogen. The difference could be due to either the significant difference in the microstructure between the alloys originating from the difference in the processing techniques or the addition of 0.11 wt.% N in this work, which is too little to significantly influence the corrosion properties of CoCrNi. Nitrogen is a well-known interstitial solid solution strengthener and contributes to the enhanced mechanical behaviour of CoCrNi.^{37,38} Preliminary results showed that with the addition of 0.11 wt.% N, yield and tensile strength increased from about 730 and 970 MPa to about 890 and 1100 MPa, respectively, while keeping the ductility >40%.³⁹ Consequently, it seems that nitrogen is a highly interesting alloying element for MEAs from both strength and corrosion properties points of view.

Now, if one compares the corrosion behaviour among different classes of alloys in this study, CoCrNi and CoCrNi-N show higher I_{corr} than 316L (both conventional and PBF-LB) in both conditions. As evident from the polarisation curves, the passivation behaviour is observed to be different for 316L alloys and MEAs. In acidic conditions, 316L fabricated using PBF-LB shows similar passivation current density as that of the MEAs, whereas in the presence of NaCl, both CoCrNi and CoCrNi-N show lower passivation current density, which infers better passivation behaviour and corrosion resistance of these MEAs. With further increase in the voltage beyond the passive region,

the corrosion of the materials proceeds through transpassive range in the acidic solution or to pitting in the presence of NaCl. The starting point for pitting could be referred to as pitting potential (E_{pit}). As observed from Figure 1B-D, E_{pit} of the CoCrNi, CoCrNi-N alloys and the 316L processed by PBF-LB are very similar, but higher than that of the 316L conventional alloy. This means that the 316L conventional alloy has the lowest resistance to pitting corrosion in comparison with the other three alloys in this study. The improved pitting and corrosion performance of PBF-LB 316L as compared with the 316L conventional alloy is attributed to the unique hierarchical microstructures and the fast solidification rate suppressing/minimising elemental segregation that would otherwise lead to coarse detrimental oxides and sulphides.^{14-16,36,40,41} All three PBF-LB materials in this study show good corrosion performance, when benchmarked against the 316L conventional alloy. Among the materials processed by PBF-LB, both MEAs show higher corrosion current density when compared with 316L. Because higher corrosion current density indicates higher corrosion rate, it is fair to assume that both MEAs have better corrosion resistance than 316L in both acidic and saline environments.

3.2 | XPS

Figure 2 illustrates the ARXPS spectra performed on all passivated samples in the present study, obtained from narrow scans at a 60° take-off angle. The fractions of hydroxide/oxide calculated from the curve fitting of O1s peaks for all the materials are also tabulated in Figure 2. The O1s signal also shows evidence of both hydroxide and oxide. As expected, the hydroxide/oxide ratio decreases as the take-off angle increases, revealing the characteristics of the passive film and the hydroxide character in the top part of both 316L and MEAs. The O1s peak fitting also shows the presence of surface moisture and S=O peak, which is due to the environment (0.5 M H₂SO₄ + 3 wt.% NaCl) in which the passivation polarisation tests were performed. It should be noted that samples were transferred in air after finishing the tests and subsequently cleaned. It is however expected that any passive film formed should not be altered upon exposure to air.

In the case of 316L alloys, it is clear from Figure 2 that the surface is covered by the Cr-Fe-oxide film, which is rich in Cr as expected. The presence of hydroxides and oxides is observed from the curve fitting from both Fe2p3 and Cr2p3 peaks. In the case of Cr, the presence of Cr₂O₃ is observed, while the curve fitting

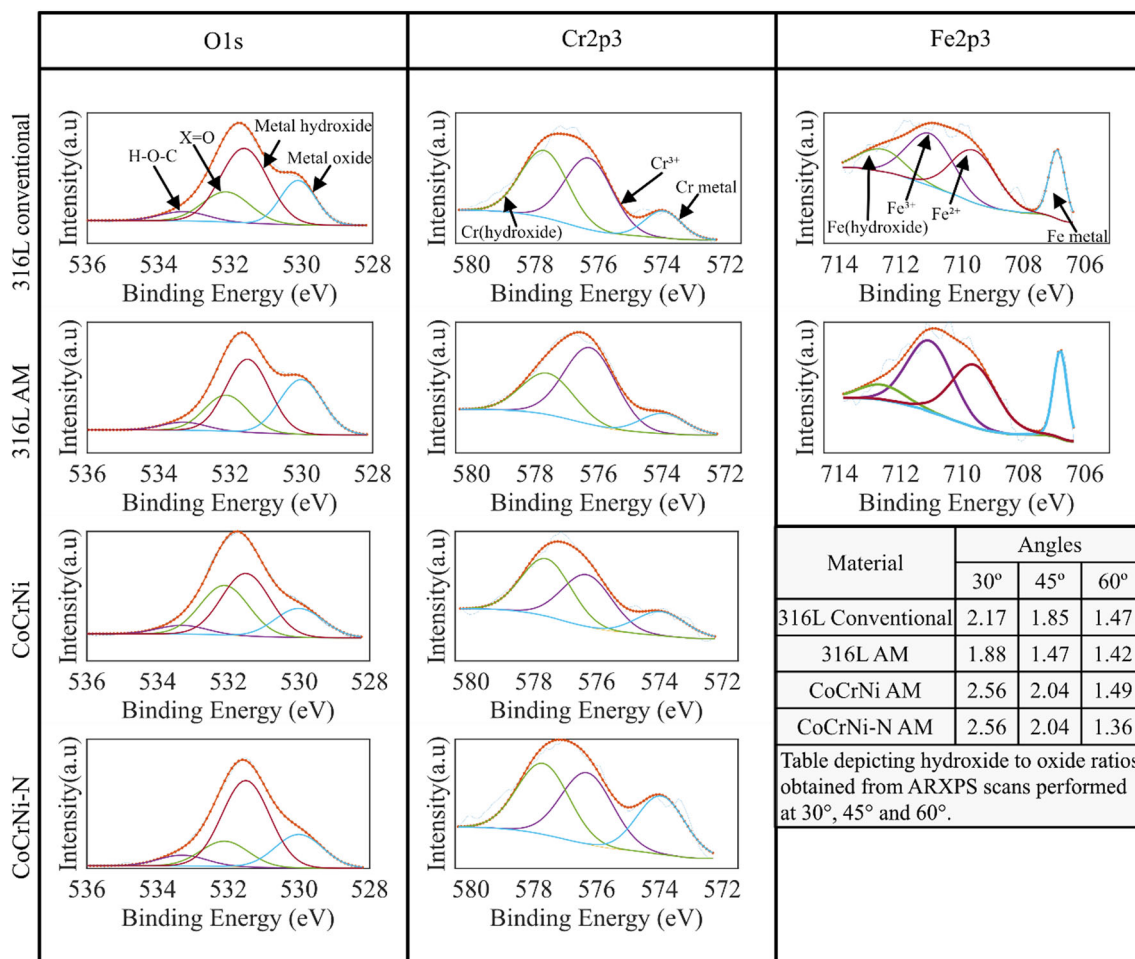


FIGURE 2 ARXPS spectra for 316L (conventional and PBF-LB) and CoCrNi and CoCrNi-N showing the original spectra and curve fitting for O1s, Cr2p and Fe2p peaks performed at a take-off angle of 60° and a table depicting the hydroxide to oxide ratios obtained from ARXPS scans performed at 30°, 45° and 60° and X in the O1s peak corresponds to fitting of both C=O and S=O.

performed on Fe shows the presence of Fe²⁺- and Fe³⁺-type oxides. At a take-off angle of 30°, metallic Fe is hardly observed, although it is clearly observed at the take-off angle of 45° (not shown in the figure). Furthermore, at higher take-off angle of 60°, stronger Fe-metal peak is also observed, indicating that increasing amount of metal is detected beneath the oxide film. The fractions of hydroxide/oxide obtained from different take-off angles show lower values for 316L manufactured through PBF-LB, as compared with its counterpart manufactured using conventional manufacturing. Moreover, the presence of sulphides is observed from XPS in the conventionally manufactured 316L, although no sulphide is observed in the 316L manufactured using PBF-LB. Mn-sulphides present in the conventionally manufactured 316L were known to be detrimental to the corrosion resistance as they could potentially dissolve in corrosive environments, creating a break in the so-formed passive layer and resulting in pitting.

CoCrNi and CoCrNi-N show similar corrosion properties in the potentiodynamic polarisation experiments in either environment (Figure 1C,D). From the XPS narrow scans on Cr, Co and Ni, only Cr

peaks are observed, which infers that only Cr takes part in the formation of the passive film. The presence of Co and Ni is not observed irrespective of the take-off angles, suggesting that the Cr₂O₃ oxide film seems to be thick enough to mitigate information from any other metallic elements than Cr. In the case of the wrought MEAs previously studied by Moravick et al.,²⁸ it was inferred that the presence of nitrogen decreased the fraction of hydroxide/oxide, resulting in the enhanced corrosion resistance. Although the hydroxide/oxide fractions calculated at different take-off angles from ARXPS show an increase in the oxide content with increasing take-off angle, very similar fractions of hydroxide/oxide are observed for both CoCrNi and CoCrNi-N (refer to the inset table in Figure 2).

4 | CONCLUSIONS

Fully dense test coupons of 316L stainless steels and two MEAs CoCrNi and CoCrNi-N, the latter with 0.11 wt.% N, were fabricated using PBF-LB. Samples were prepared for potentiodynamic

polarisation studies and compared with the conventionally manufactured 316L as a benchmark. To correlate the corrosion testing with surface chemical compositions, samples anodically polarised to the passive range were analysed by ARXPS. The main findings can be summarised as follows.

- The AM-fabricated 316L shows better corrosion properties than the conventional 316L used as benchmark in the current study. On all measures like free corrosion potential, corrosion current density, passivation current density and in particular passivation current density, the AM-fabricated 316L shows superior performance.
- The AM-fabricated MEAs CoCrNi and CoCrNi-N show attractive corrosion properties, with free corrosion potential and corrosion current density better than the AM-fabricated 316L.
- Compared with the conventionally manufactured 316L, the AM-processed material shows better corrosion properties in the pitting corrosion environment such as 0.5 M H₂SO₄ + 3 wt.% NaCl. The actual mechanism will be subject to further studies. However, it could be anticipated that even if AM generally means incorporation of nm-size oxide inclusions (formed from powder surface oxide), these inclusions are suggested to not be harmful to the corrosion properties, whereas the conventionally manufactured 316L contains MnS inclusions, which are supposedly detrimental to its pitting corrosion resistance.
- The XPS analyses confirms that the passive film on the AM-fabricated 316L consists of Cr-Fe oxide, rich in Cr. Also, in line with the behaviour of stainless steels, the passive film is found to be a mixture of hydroxide/oxide with higher hydroxide content on the top surface.
- For both CoCrNi and CoCrNi-N alloys, a mixture of Cr oxides and Cr hydroxides are observed. This is supposed to be a result of the fact that both Co and Ni act as the noble alloying elements and they do not take part in the oxide film formation.

ACKNOWLEDGEMENTS

This study was done as part of the Competence Centre for Additive Manufacturing – Metals (CAM2) (Grant No. 2016-05175) by Swedish Innovation Agency and the European Union's Horizon 2020 research and innovation programme within project MANUELA-Additive Manufacturing Using Metal Pilot Line (Grant No. 820774). Support from the Production Area of Advance at Chalmers and technical co-operation with Höganäs AB is gratefully acknowledged, including the co-operation and contributions from Adjunct Professors Karin Frisk and Sven Bengtsson.

DATA AVAILABILITY STATEMENT

Data available on request from the authors.

ORCID

Sri Bala Aditya Malladi  <https://orcid.org/0000-0001-5704-802X>

Yu Cao  <https://orcid.org/0000-0002-1965-5854>

Lars Nyborg  <https://orcid.org/0000-0002-1726-5529>

REFERENCES

1. Herzog D, Seyda V, Wycisk E, Emmelmann C. Additive manufacturing of metals. *Acta Mater*. 2016;117:371-392. doi:10.1016/j.actamat.2016.07.019
2. Frazier WE. Metal additive manufacturing: a review. *J Mater Eng Perform*. 2014;23(6):1917-1928. doi:10.1007/s11665-014-0958-z
3. Emmelmann C, Kranz J, Herzog D, Wycisk E. *Laser Additive Manufacturing of Metals*. Berlin, Heidelberg: Springer; 2013:143-162. doi:10.1007/978-3-642-41341-4_6
4. Jia H, Sun H, Wang H, Wu Y, Wang H. Scanning strategy in selective laser melting (SLM): a review. *Int J Adv Manuf Technol*. 2021; 113(9-10):2413-2435. doi:10.1007/s00170-021-06810-3
5. Zhang X, Yocom CJ, Mao B, Liao Y. Microstructure evolution during selective laser melting of metallic materials: a review. *J Laser Appl*. 2019;31(3):031201. doi:10.2351/1.5085206
6. Yadroitsev I, Smurov I. Selective laser melting technology: from the single laser melted track stability to 3D parts of complex shape. *Phys Procedia*. 2010;5(PART 2):551-560. doi:10.1016/j.phpro.2010.08.083
7. Gong X, Chou K. Microstructures of Inconel 718 by selective laser melting. In: *TMS 2015 144th Annual Meeting & Exhibition*. Springer; 2015:461-468. doi:10.1007/978-3-319-48127-2_58
8. Basak A, Das S. Epitaxy and microstructure evolution in metal additive manufacturing. *Annu Rev Mat Res*. 2016;46(1):125-149. doi:10.1146/annurev-matsci-070115-031728
9. Durga A, Pettersson NH, Malladi SBA, et al. Grain refinement in additively manufactured ferritic stainless steel by in situ inoculation using pre-alloyed powder. *Scr Mater*. 2021;194:113690. doi:10.1016/j.scriptamat.2020.113690
10. Liverani E, Toschi S, Ceschini L, Fortunato A. Effect of selective laser melting (SLM) process parameters on microstructure and mechanical properties of 316L austenitic stainless steel. *J Mater Process Technol*. 2017;249:255-263. doi:10.1016/J.JMATPROTEC.2017.05.042
11. Sander G, Tan J, Balan P, et al. Corrosion of additively manufactured alloys: a review. *Corrosion*. 2018;74(12):1318-1350. doi:10.5006/2926
12. Örnek C. Additive manufacturing – a general corrosion perspective. *Corros Eng Sci Technol*. 2018;53(7):531-535. doi:10.1080/1478422X.2018.1511327
13. Kale AB, Kim BK, Kim DI, Castle EG, Reece M, Choi SH. An investigation of the corrosion behavior of 316L stainless steel fabricated by SLM and SPS techniques. *Mater Charact*. 2020;163:110204. doi:10.1016/J.MATCHAR.2020.110204
14. Andreatta F, Lanzutti A, Vaglio E, Totis G, Sortino M, Fedrizzi L. Corrosion behaviour of 316L stainless steel manufactured by selective laser melting. *Werkst Korros*. 2019;70(9):1633-1645. doi:10.1002/MACO.201910792
15. Geenen K, Röttger A, Theisen W. Corrosion behavior of 316L austenitic steel processed by selective laser melting, hot-isostatic pressing, and casting. *Werkst Korros*. 2017;68(7):764-775. doi:10.1002/MACO.201609210
16. Revilla RI, van Calster M, Raes M, et al. Microstructure and corrosion behavior of 316L stainless steel prepared using different additive manufacturing methods: a comparative study bringing insights into the impact of microstructure on their passivity. *Corros Sci*. 2020;176: 108914. doi:10.1016/J.CORSCI.2020.108914
17. Kazempour M, Mohammadi M, Mfoumou E, Nasiri AM. Microstructure and corrosion characteristics of selective laser-melted 316L stainless steel: the impact of process-induced porosities. *JOM*. 2019; 71(9):3230-3240. doi:10.1007/S11837-019-03647-W
18. Leicht A, Fischer M, Klement U, Nyborg L, Hryha E. Increasing the productivity of laser powder bed fusion for stainless steel 316L through increased layer thickness. *J Mater Eng Perform*. 2021;30(1): 575-584. doi:10.1007/S11665-020-05334-3/FIGURES/10

19. Riabov D, Cordova L, Hryha E, Bengtsson S. Effect of powder variability on laser powder bed fusion processing and properties of 316L. *EJMS*. 2022;2(1):202-221. doi:[10.1080/26889277.2022.2064772](https://doi.org/10.1080/26889277.2022.2064772)
20. Sun Z, Tan X, Tor SB, Chua CK. Simultaneously enhanced strength and ductility for 3D-printed stainless steel 316L by selective laser melting. *NPG Asia Mater*. 2018;10(4):127-136. doi:[10.1038/s41427-018-0018-5](https://doi.org/10.1038/s41427-018-0018-5)
21. Tsai MH, Yeh JW. High-entropy alloys: a critical review. *Mater Res Lett*. 2014;2(3):107-123. doi:[10.1080/21663831.2014.912690](https://doi.org/10.1080/21663831.2014.912690)
22. George EP, Raabe D, Ritchie RO. High-entropy alloys. *Nat Rev Mater*. 2019;4(8):515-534. doi:[10.1038/s41578-019-0121-4](https://doi.org/10.1038/s41578-019-0121-4)
23. Guo S, Hu Q, Ng C, Liu CT. More than entropy in high-entropy alloys: forming solid solutions or amorphous phase. *Intermetallics*. 2013;41:96-103. doi:[10.1016/j.intermet.2013.05.002](https://doi.org/10.1016/j.intermet.2013.05.002)
24. Gludovatz B, Hohenwarter A, Thurston KVS, et al. Exceptional damage-tolerance of a medium-entropy alloy CrCoNi at cryogenic temperatures. *Nat Commun*. 2016;7(1):10602. doi:[10.1038/ncomms10602](https://doi.org/10.1038/ncomms10602)
25. Zhang Z, Sheng H, Wang Z, et al. Dislocation mechanisms and 3D twin architectures generate exceptional strength-ductility-toughness combination in CrCoNi medium-entropy alloy. *Nat Commun*. 2017;8(1):1-8. doi:[10.1038/ncomms14390](https://doi.org/10.1038/ncomms14390)
26. Shang X, Wang Z, Feng HE, Wang J, Li J, Jiakang YU. The intrinsic mechanism of corrosion resistance for FCC high entropy alloys. *Sci China Technol Sci*. 2018;61(2):189-196. doi:[10.1007/s11431-017-9114-1](https://doi.org/10.1007/s11431-017-9114-1)
27. Qiu Y, Thomas S, Gibson MA, Fraser HL, Birbilis N. Corrosion of high entropy alloys. *NPJ Mater Degrad*. 2017;1(1):1-18. doi:[10.1038/s41529-017-0009-y](https://doi.org/10.1038/s41529-017-0009-y)
28. Moravcik I, Peighambardoust NS, Motalebzadeh A, et al. Interstitial nitrogen enhances corrosion resistance of an equiatomic CoCrNi medium-entropy alloy in sulfuric acid solution. *Mater Charact*. 2021;172:110869. doi:[10.1016/J.MATCHAR.2020.110869](https://doi.org/10.1016/J.MATCHAR.2020.110869)
29. Mohamed O, Hassan M, Egilmez M, Abuzaid W, Ibrahim T, Khamis M. Corrosion behavior of CoCrNi/mild steel medium entropy alloy thin films. *Mater Today Commun*. 2022;30:103015. doi:[10.1016/J.MTCOMM.2021.103015](https://doi.org/10.1016/J.MTCOMM.2021.103015)
30. Wang J, Li W, Yang H, et al. Corrosion behavior of CoCrNi medium-entropy alloy compared with 304 stainless steel in H2SO4 and NaOH solutions. *Corros Sci*. 2020;177:108973. doi:[10.1016/J.CORSCI.2020.108973](https://doi.org/10.1016/J.CORSCI.2020.108973)
31. Korde JM, Sreekumar AV, Kandasubramanian B. Corrosion inhibition of 316L-type stainless steel under marine environments using epoxy/waste plastic soot coatings. *SN Appl Sci*. 2020;2(7):1-13. doi:[10.1007/S42452-020-3096-2/FIGURES/9](https://doi.org/10.1007/S42452-020-3096-2/FIGURES/9)
32. Dhaiveegan P, Elangovan N, Nishimura T, Rajendran N. Corrosion behavior of 316L and 304 stainless steels exposed to industrial-marine-urban environment: field study. *RSC Adv*. 2016;6(53):47314-47324. doi:[10.1039/C6RA04015B](https://doi.org/10.1039/C6RA04015B)
33. Zhu M, He F, Yuan Y, Guo S, Wei G. A comparative study on the corrosion behavior of CoCrNi medium-entropy alloy and 316L stainless steel in simulated marine environment. *Intermetallics*. 2021;139:107370. doi:[10.1016/J.INTERMET.2021.107370](https://doi.org/10.1016/J.INTERMET.2021.107370)
34. Krawiec H, Vignal V, Heintz O, Oltra R, Olive JM. Influence of the chemical dissolution of MnS inclusions on the electrochemical behavior of stainless steels. *J Electrochem Soc*. 2005;152(7):B213. doi:[10.1149/1.1924172](https://doi.org/10.1149/1.1924172)
35. Yue X, Yang Z, Huang L, et al. Passivation characteristics of ultra-thin 316L foil in NaCl solutions. *J Mater Sci Technol*. 2022;127:192-205. doi:[10.1016/j.jmst.2022.01.043](https://doi.org/10.1016/j.jmst.2022.01.043)
36. Chao Q, Cruz V, Thomas S, et al. On the enhanced corrosion resistance of a selective laser melted austenitic stainless steel. *Scr Mater*. 2017;141:94-98. doi:[10.1016/J.SCRIPTAMAT.2017.07.037](https://doi.org/10.1016/J.SCRIPTAMAT.2017.07.037)
37. Moravcik I, Hornik V, Minárik P, et al. Interstitial doping enhances the strength-ductility synergy in a CoCrNi medium entropy alloy. *Mater Sci Eng a*. 2020;781:139242. doi:[10.1016/J.MSEA.2020.139242](https://doi.org/10.1016/J.MSEA.2020.139242)
38. Moravcik I, Hadraba H, Li L, Dlouhy I, Raabe D, Li Z. Yield strength increase of a CoCrNi medium entropy alloy by interstitial nitrogen doping at maintained ductility. *Scr Mater*. 2020;178:391-397. doi:[10.1016/J.SCRIPTAMAT.2019.12.007](https://doi.org/10.1016/J.SCRIPTAMAT.2019.12.007)
39. Sri Bala Aditya M. Microstructural development in laser-based powder bed fusion-from ferritic stainless steel to medium entropy alloys. Licentiate dissertation, Chalmers University of Technology. 2021; IMS-2021(22).
40. Williams DE, Kilburn MR, Cliff J, Waterhouse GIN. Composition changes around sulphide inclusions in stainless steels, and implications for the initiation of pitting corrosion. *Corros Sci*. 2010;52(11):3702-3716. doi:[10.1016/J.CORSCI.2010.07.021](https://doi.org/10.1016/J.CORSCI.2010.07.021)
41. Ryan MP, Williams DE, Chater RJ, Hutton BM, McPhail DS. Why stainless steel corrodes. *Nature*. 2002;415(6873):770-774. doi:[10.1038/415770a](https://doi.org/10.1038/415770a)

How to cite this article: Malladi SBA, Tam PL, Cao Y, Guo S, Nyborg L. Corrosion behaviour of additively manufactured 316L and CoCrNi. *Surf Interface Anal*. 2023;1-7. doi:[10.1002/sia.7200](https://doi.org/10.1002/sia.7200)